Magnesium Imidazolate Borohydride Complex: A New Type of Hybrid Material

Journal:	*Inorganic Chemistry*
Manuscript ID	ic-2022-013192
Manuscript Type:	Article
Date Submitted by the Author:	23-May-2022
Complete List of Authors:	Reberc, Maja; University of Ljubljana Faculty of Chemistry and Chemical Technology, Department of Chemistry and Biochemistry Mazaj, Matjaz; Kemijski institut, Stare, Jernej; Kemijski institut, Počkaj, Marta; University of Ljubljana Faculty of Chemistry and Chemical Technology, Department of Chemistry and Biochemistry Mali, Gregor; Kemijski institut, Department of Inorganic Chemistry and Technology Li, Xiao; Université catholique de Louvain, Institute of Condensed Matter and Nanosciences Filinchuk, Yaroslav; Universite catholique de Louvain, Institute of Condensed Matter and Nanosciences Černý, Radovan; University of Geneva, Department of Quantum Matter Physics Meden, Anton; University of Ljubljana Faculty of Chemistry and Chemical Technology, Department of Chemistry and Biochemistry

Magnesium Imidazolate Borohydride Complex: A New Type of Hybrid Material

Maja Reberc,[†] Matjaž Mazaj,[‡] Jernej Stare,[‡] Marta Počkaj,[†] Gregor Mali,[‡] Xiao Li,[¶] Yaroslav Filinchuk,[¶] Radovan Černý,[§] and Anton Meden*[,†]

[†]*Faculty of Chemistry and Chemical Technology, University of Ljubljana, Večna pot 113, 1001 Ljubljana, Slovenia*

[‡]*National Institute of Chemistry, Hajdrihova 19, 1000 Ljubljana, Slovenia*

[¶]*IMCN Université Catholique de Louvain, Place L. Pasteur 1, B-1348, Louvain-la-Neuve, Belgium*

[§]*DQMP, University of Geneva, 24 quai Ernest-Ansermet, 1211 Geneva, Switzerland*

E-mail: anton.meden@fkkt.uni-lj.si

Abstract

A new type of hybrid compound, combining properties of MOFs and borohydrides, was synthesized solvothermally using $Mg(BH_4)_2$ and imidazole as precursors. Material in the form of acetonitrile solvate with formula $[Mg_3\{(Im)BH_2(Im)\}_6(ImH)_6]\cdot CH_3CN$ crystallizes in the space group $R\bar{3}$, having the unit cell parameters $a = 15.1942(2)$ Å and $c = 28.3157(3)$ Å as determined by single crystal X-ray diffraction. The structure was further investigated by solid state NMR and DFT quantum chemical calculations. The main feature of the structure, reported here for the first time, is a linear trinuclear complex, where octahedrally nitrogen-coordinated Mg^{2+} ions are bridged with $\{(Im)BH_2(Im)\}^-$ units, forming inside voids of 4.6 Å in diameter between the magnesium ions. Polar intermolecular interactions hold the molecules in a dense

rhombohedral stacking, where a disordered acetonitrile molecule plays a cohesive role. The compound is stable in air and upon heating to about 160 °C. Using an alternative synthesis method from imidazole melt, an imidazole solvate with the formula $[Mg_3\{(Im)BH_2(Im)\}_6(ImH)_6] \cdot ImH$ and a very similar crystal structure to acetonitrile solvate was prepared. It is stable up to 220 °C. Upon further heating, it transformed into a layered structure with the formula $Mg(Im_3BH)_2$, space group $P\bar{3}1c$, and unit cell parameters $a = 8.7442(4)$ Å, $c = 17.643(2)$ Å determined by synchrotron powder diffraction. Besides its structural novelty, two types of potentially reactive hydrogens, bonded to boron and nitrogen in the same molecule, make the material highly interesting for future investigations in the fields of energy storage applications.

Introduction

The research of hybrid organic-inorganic systems experienced an immense interest in recent decades. The integration of organic and inorganic moieties either on atomic or macroscopic scale can namely synergistically improve the physicochemical properties or even generate features that individual components do not possess. Therefore this concept resulted in development of numerous advanced materials which are considered to be the state-of-the-art in the fields of catalysis,[1–5] bioapplications,[3,6–9] electrochemistry,[10,11] sensoring[12,13] and energy performance.[14–16] Among energy storage processes, hydrogen is considered as one of the most promising energy carriers as an alternative to fossil fuels. The biggest challenge, however, represents its storage under low-cost and safe conditions. In that manner, the development of solid materials that would capture hydrogen via physisorption or chemisorption providing sufficiently high gravimetric and volumetric density of hydrogen and suitable adsorption/desorption thermodynamics and kinetics still remains a great obstacle. Most frequently studied materials for adsorption of hydrogen are metal-organic frameworks (MOFs) and metal-based hydrides/borohydrides.[17] MOFs can on one hand possess low-density structures with highly accessible pore system and tunable structure functionality, however major-

ity of the developed MOF systems still suffer from low mass and volume capacity of hydrogen at ambient conditions due to the weak framework-to-hydrogen interactions. On the other hand borohydrides can contain sufficient amounts of hydrogen even at room temperature and pressure, but its covalent bonding inhibits the efficiency of desorption and makes this process irreversible. The possible solution that could overcome the drawbacks of both types of materials is the development of hybrid architectures containing the structural features of both metal borohydrides and metal-organic frameworks. Nanoparticles of various metal borohydrides have already been confined within MOF structures resulting in improved energy efficiency of the intrinsic borohydride dehydrogenation[18–20] which can either enhance the hydrogen release at lower temperatures[21] or generate catalytically active reducing sites within MOF frameworks.[20,22,23] However, nanoconfined metal borohydride/MOF composites contain in most cases 'extra-framework' borohydride species applied within MOF matrices mostly under post-synthesis conditions establishing relatively weak van der Waals-type interactions to matrix frameworks. This can importantly affect the durability of the sorption or catalytic system.

Many structures containing boron atoms, bound to the one of nitrogen atoms of the imidazolate units in their frameworks, have already been reported. Most of them belong to a subset of MOFs, named BIFs (boron imidazolate frameworks).[24] These structures feature three or four imidazolate anions or their derivates bound to boron centers via one of the nitrogen atoms, having various mono- and divalent metal cations coordinated to the other nitrogen atom of the imidazolate. Only in the case of trisubstituted boron imidazolates of this kind, containing the unit, $BH(Im)_3^-$, one of the potentially reactive hydrides, bound to boron, is preserved.

Searching for metal imidazolates hydridoborates with more than one hydride bound to boron in the CSD[25] revealed very little results. Two hydrides bound to boron are present only in two structures (QUESTIR and QUESTUD).[26] In both of them the metal atom is silver and imidazolate is unsubstituted (hydrogen atom is bound to each of the three

carbon atoms). QUESTIR is a chain coordination polymer, while QUESTUD contains cyclic molecular units. No structure of this type with three hydrides bound to boron was found, and only three structures with co-existing tetrahydridoborate and a metal, coordinated to the N atom of an imidazole, could be found in the CSD. These are molecular NUFXOD,[27] chain SOHHEF[18] and molecular SUMZEG.[28] In all cases the imidazole is (at least) N-substituted and neutral, while the metal cations are Co(II), Mn(II) and Li(I), respectively.

The first compound with simultaneous presence of deprotonated imidazolate, acting as N-donor ligand, and tetrahydridoborate was prepared in 2017 by Morelle, who synthesized the compound Li_2ImBH_4. It has three known polymorphic forms, all showing extended (layer or framework) structural features.[29] Besides that, similar derivatives were obtained from $LiBH_4$ and methyl- and benzimidazolates of Li. To our knowledge, these three compounds are the only known of such kind up to now. The compound with benzimidazolate, $Li_2(bIm)BH_4$, shows remarkable dynamics of groups (rotational tunneling), favored by its unusual environment.[30]

During efforts to produce similar compounds with other light metals, we were able to synthesize a previously unknown molecular compound, which is reported in this work. Since the compound is new, most efforts were devoted to thorough structural characterization, using single crystal X-ray diffraction, solid state NMR and quantum chemical calculations as we wanted to well define the identity of the new material and provide the basis for understanding its properties. In addition, we aimed to determine some basic physico-chemical properties of the novel compound as are the stability in air, thermal stability and sorption properties.

In search of an alternative method of synthesis with the intention of producing a solvent-free form of the title compound, a procedure using molten imidazole was found. It, interestingly, resulted in an imidazole solvate, which we also report here.

Experimental Section

Material Synthesis

The compound in the form of acetonitrile solvate was prepared using the solvothermal synthesis method inside a glove box with nitrogen atmosphere. Magnesium borohydride ($Mg(BH_4)_2$, Sigma-Aldrich, 95 %), imidazole (ImH, Sigma-Aldrich, ≥99 %) and acetonitrile (CH_3CN, Sigma-Aldrich, 99.8 %, dried over CaH_2) were added to a 23 mL teflon-lined stainless steel autoclave, which was then heated in an oven at 85 °C for 24 h. The product was centrifuged at 5000 rpm for 5 min in the glove box. The supernatant was decanted and fine white powder was obtained. After the remaining solvent evaporated from the teflon liner, colorless crystals formed on its surface. A more detailed description of the procedure and investigated reactant ratios are available in the Supporting Information.

Another procedure that allows to avoid the use of autoclaves and solvents, aiming to produce a solvent-free compound, was subsequently developed, namely, synthesis in imidazole melt. It was found that this product is not solvent-free. However, it is different from the acetonitrile solvate and it is therefore worth reporting its synthesis. γ-$Mg(BH_4)_2$ (272 mg, 5 mmol) and imidazole (2720 mg, 40 mmol) were loaded into a modified Schlenk flask in a glove box with argon atmosphere. The flask was connected to the Schlenk line and the mixture was heated in flow of argon in an oil bath until the solid imidazole was molten at about 70–85 °C. Reaction was manifested by the evolution of hydrogen in form of bubbles. The temperature of the reaction mixture was kept at 110 °C for 20 h. The heating was stopped and the product was washed with tetrahydrofuran (THF) while hot, aiming to remove the excess imidazole. 20 mL of THF was used at first, and then the product was rinsed 3 more times with 8 mL of THF. The product was dried under vacuum at room temperature.

Structural Characterization

Single-crystal X-ray diffraction. A single crystal of the title compound in the form of acetonitrile solvate was dipped into silicon grease and mounted onto the tip of a glass fiber and transferred to the goniometer head, under a nitrogen cryostream. Data were collected on a SuperNova diffractometer equipped with an Atlas detector, using CrysAlis PRO software, and monochromated CuKα radiation (1.541 84 Å) at 150 K.[31] The initial structural model containing the coordination molecule was obtained using the Superflip structure solution program.[32] Full-matrix least-squares refinement on F^2 with anisotropic displacement parameters for all nonhydrogen atoms was carried out using *SHELXL*-2018/3.[33] All H atoms were initially located in difference Fourier maps and were further treated as riding on their parent atoms with C(aromatic)–H = 0.95 Å. Hydrogens, bonded to B, were refined freely, while the N–H bonds were restrained to 0.87(2) Å.

The atoms forming the acetonitrile molecules were observed in the difference Fourier maps. The obtained molar ratio between $[Mg_3\{(Im)BH_2(Im)\}_6(ImH)_6]$ and acetonitrile molecules was 1:1. The central atom of the acetonitrile, C11, resided on an inversion center positioned on a threefold inversion axis, which lead to severe symmetry-induced disorder of the acetonitrile molecules with ill-defined bond lengths and angles, and precluded the location of hydrogen atoms. Consequently, the coordinates of acetonitrile molecule were taken from the results of quantum chemical calculations, from the model with the lowest potential energy, and they were fixed in the last refinement cycles while atomic displacement parameters of all acetonitrile atoms were refined isotropically. In the trials to refine the ADPs of the acetonitrile atoms anisotropically, some of them became non-positive definite. For the acetonitrile hydrogens, their isotropic displacement parameters were restrained to be 1.5-times larger than that of their carrier atom's.

Figures depicting the structure were prepared with Mercury.[34] Details on crystal data, data collection and structure refinement, as well as data on selected bond lengths and angles, are given in the Supporting Information.

Crystal structure optimizations. Periodic DFT calculations were employed for the assessment of various aspects of the structure of the title system in the form of acetonitrile solvate. Optimization of the structures was carried out by the VASP 5.3.5 program package[35–38] using the revised version[39] of the Perdew-Burke-Ernzerhof functional,[40] corrected for dispersion interactions by the zero damping DFT-D3 method of Grimme,[41] plane-wave basis set with a kinetic energy cutoff of 500 eV, Projector Augmented Wave atomic pseudopotentials,[42,43] and Monkhorst-Pack[44] k-point mesh of $2 \times 2 \times 1$ points. Structures subject to optimization were built on the basis of the present crystal structure solution by using the CIF2Cell utility.[45] Various optimization strategies were imposed, differing mainly in fixation/relaxation of unit cell parameters and adjusting optimization step width scaling constant. When using fixed unit cell parameters, the corresponding values were set to those obtained by diffraction.

Crystal structure of the title system was found to contain disordered molecules of solvent acetonitrile, with the central carbon atom of the linear C-C-N moiety positioned nearly on a threefold inversion axis. According to crystallography, this would generate six different orientations of the molecule. The CH_3CN molecule is linear and from the results of X-ray diffraction it could be concluded that it is not perpendicular to the threefold axis but encloses an angle of about 80° with it. The threefold inversion axis first generates two additional molecules in increments of 120°. All three crystallographically equivalent molecules are then inverted by the same symmetry element, bringing the terminal C atom nearly over the N atom and vice versa. From the view along the threefold inversion axis, it looks as having six molecules in increments of 60°, forming a hexagon, while the side view reveals that three of them have an inclination to the threefold axis of about 80°, and the other three are inclined by about 100°. All six orientations were investigated with calculations. Accordingly, crystal structures corresponding to these orientations (oriented identically in all three occurrences in the unit cell) were prepared in space group P1 and optimized using the settings given above. Additionally, all solvent molecules were removed from the crystal structure, which was then

optimized, focusing on the change in intermolecular interactions and in the density. Finally, a single acetonitrile molecule in vacuum and structure model with acetonitrile molecules removed were optimized separately to estimate interaction energy of acetonitrile with the rest of the structure. The acetonitrile molecule was placed in a cubic box of 20 Å. Periodicity was still imposed, but the large size of the box ensures that intermolecular interactions become vanishingly small, thereby reasonably mimicking a vacuum model.

Prior to above calculations, a structure with a single orientation of acetonitrile molecules and an identical model structure with acetonitrile molecules removed were optimized using three different functionals: the original Perdew-Burke-Ernzerhof[40] (PE), its revised version[39] (RP) and a version specially tuned for solids[46] (PS). Of those, functional RP was identified as optimal on the criterion of match between optimized and experimental unit cell parameters (Table S4 in Supporting Information) and was used for all following calculations.

Rietveld analysis of powder patterns. Rietveld analysis was performed using TOPAS-Academic V7.[47] The structural model of the $[Mg_3\{(Im)BH_2(Im)\}_6(ImH)_6]$ moiety was constructed in the form of a Z-matrix based on the crystal structure determined by single-crystal X-ray diffraction. The acetonitrile and imidazole molecules and the $[BIm_3H]$ moiety were also constructed in the form of Z-matrices using the interatomic distances and angles found for similar fragments in the CSD. The orientations and positions of the solvent molecules were freely refined, as was the rotation of the $[Mg_3\{(Im)BH_2(Im)\}_6(ImH)_6]$ moiety about the threefold axis, while the position and orientation of the latter along the axis were constrained by keeping the central magnesium atom on the inversion center at the threefold axis and the other two Mg atoms (which are symmetry equivalents) on the threefold axis but off the inversion center. All distances, angles, and dihedral angles were then refined with restrictions that kept the molecular geometries within acceptable limits, derived from the structures of similar fragments found in the CSD. For more details, see the Supporting Information.

Liquid-state NMR. Nuclear magnetic resonance (NMR) spectrum of the imidazole solvate was measured on a Bruker 500 UltraShield spectrometer. The compound was dissolved

in deuterated water (D_2O) and immediately characterized by ^{11}B NMR spectroscopy.

Solid-state NMR. Solid-state NMR spectra of the title system in the acetonitrile solvate form were measured on a 600 MHz Varian VNMRS spectrometer, equipped with a 1.6 mm HXY CPMAS probe. Larmor frequencies for ^{1}H, ^{11}B and ^{13}C nuclei were 599.51 MHz, 192.34 MHz and 150.76 MHz, respectively. All measurements, except ^{1}H MAS NMR measurement, were carried out at sample rotation frequency of 20 kHz. ^{1}H MAS NMR spectrum was obtained at sample rotation frequency of 40 kHz, using a 90-degree excitation pulse of 1.4 µs and repetition delay of 10 s. ^{11}B MAS NMR measurement employed a short 0.8 µs excitation pulse and high-power XiX proton decoupling during acquisition; 128 scans were collected and delay between the scans was 10 s. ^{1}H-^{13}C LG-CPMAS experiment used Lee-Goldburg cross-polarization scheme with duration of 100 µs and high-power proton decoupling; repetition delay was 2 s and number of scans was 4800. In both 2D HETCOR experiments spectral width and number of increments in the indirect dimension were 20 kHz and 20, respectively, XiX decoupling was used and repetition delay was 2 s. For the measurement of the ^{1}H-^{11}B HETCOR spectrum a constant-amplitude cross-polarization block of 80 µs was used and number of scans was 40; for the ^{1}H-^{13}C HETCOR ramped-amplitude cross-polarization block of 2 ms was employed (ramp on the proton channel) and number of scans was 800. Chemical shifts of ^{1}H and ^{13}C nuclei were reported relative to the corresponding signals of tetramethylsilane, whereas the ^{11}B chemical shift axis was set using 1 M solution of H_3BO_3 in water as a secondary reference (^{11}B nuclei resonate at 19.6 ppm).

NMR calculations. First-principles calculations of chemical-shielding and quadrupolar-coupling parameters were carried out with the GIPAW/DFT approach using CASTEP software package (Materials Studio v. 5.5.3, Accelrys Software Inc.). Two different structural models were derived from the XRD-based model, one without acetonitrile molecules and with $R\bar{3}$ space group, and one with acetonitrile molecules and with space group P1. Both structural models were geometry optimized with the DFT-based structure relaxation. Plane-wave basis, generalized gradient approximation of Perdew-Burke-Ernzerhof, and ultrasoft pseu-

dopotentials (generated on-the-fly with CASTEP) were employed. Two runs of geometry optimizations were carried out for each model, one with and one without allowing the variation of the unit cell parameters. Upon optimization, force on each atom was smaller than 0.08 eV/Å and stress was below 0.1 GPa. In the DFT-based structure relaxation, kinetic-energy cutoff for the plane-wave basis was set to 600 eV, and the reciprocal-space sampling was performed with the k-point grid spacing of 0.1 $Å^{-1}$ or less. For the calculations of chemical shifts and quadrupolar coupling constants the kinetic-energy cutoff for the plane-wave basis was increased to 700 eV and k-point grid spacing was decreased below 0.05 $Å^{-1}$. GIPAW calculations yielded isotropic chemical shielding σ^{iso}, from which isotropic chemical shift was obtained as $\delta_{\mathrm{CS}}^{\mathrm{iso}} = \sigma^{\mathrm{ref}} - \sigma^{\mathrm{iso}}$. Here σ^{ref} was 168 ppm for ^{13}C and 30 ppm for ^{1}H nuclei. Agreement between the calculated and the experimentally determined chemical shifts was slightly better for structural models, in which only variation of atomic coordinates was allowed.

Stability, Morphology, Purity and Sorption Measurements

Scanning electron microscopy. SEM observations were performed on a Zeiss Supra 3VP field-emission gun scanning electron microscope (FEG-SEM).

Powder X-ray diffraction. Samples of the acetonitrile solvate were finely ground and loaded in glass capillaries (Hilgenberg, diameter 0.7 mm), which were broken off above sample level and sealed with modeling clay. Measurements in transmission geometry were carried out with PANalytical X'Pert Pro MPD powder diffractometer using CuKα_1 radiation (45 kV, 40 mA) in the range 7–33 °2θ with step time 800 s and step size 0.05 °2θ. Powder phase and predominantly single-crystal phase of most syntheses were analyzed separately. In addition, a powdered sample was analyzed after 29 days of exposure to air to study stability of the title compound. Reflection geometry with CuK$\alpha_{1,2}$ radiation (45 kV, 40 mA) was used in range 3–50 °2θ with step time 100 s and step size 0.034 °2θ.

Temperature-programmed X-ray powder diffraction pattern of powdered sample of the

acetonitrile solvate was recorded also on the PANalyticalX'Pert PRO diffractometer additionally equipped with a high-temperature sample cell, from room temperature to 700 °C in steps of 20 °C in static air.

All temperature-programmed measurements of the imidazole solvate of the title compound were done at SNBL/ESRF. Pilatus 2M detector was used with wavelength 0.728 030 Å.

Thermal analysis. The thermal gravimetric analysis (TGA) was performed using a Q5000 IR thermogravimeter (TA Instruments, Inc.). The measurements were carried out in an airflow (10 mL/min) with a heating rate of 10 °C/min.

Infrared spectroscopy. A powdered sample was exposed to air and periodically analyzed by infrared spectroscopy to study stability. The spectra were acquired using Bruker Alpha II and PerkinElmer Spectrum Two FTIR spectrometers in ATR configuration.

Sorption measurements. N_2 and H_2 sorption isotherms were measured with an HTP-IMI analyzer (Hiden Isochema Inc.). Before the measurements, the sample was outgassed at 50 °C for 2 h.

Results and Discussion

Synthesis

Borohydride-type materials are usually produced with the lack of solvent using mechanochemical process due to the reactivity of borohydride precursors yielding only finely powdered products. Such approach therefore makes the structure analysis more difficult. The facile solvothermal approach described herein enables the growth of larger crystals suitable for single-crystal structure analysis.

Product with the formula $[Mg_3\{(Im)BH_2(Im)\}_6(ImH)_6] \cdot CH_3CN$ and rather large crystallites was synthesized from $Mg(BH_4)_2$, ImH and CH_3CN in molar ratio of 1:15:680 (15.2 mg, 287.5 mg and 10 mL, respectively) with yield of 55 % referring to $Mg(BH_4)_2$. A SEM micrograph of a crystal obtained is shown in the Supporting Information.

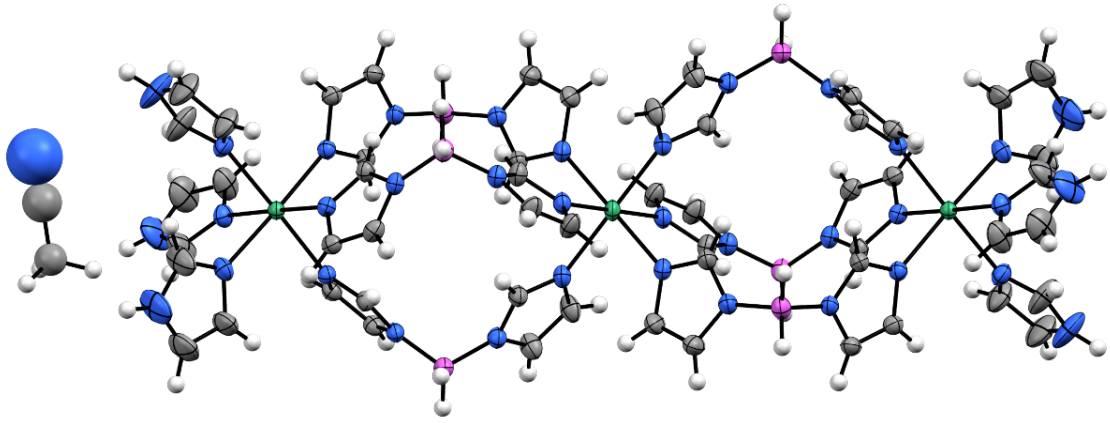

Figure 1: Structure of the $[Mg_3\{(Im)BH_2(Im)\}_6(ImH)_6]$ molecule and disordered acetonitrile (only one of six acetonitrile symmetry-related overlapping positions is shown for clarity). Mg atoms – green, N atoms – blue, C atoms – gray, B atoms – pink, H atoms – white.

The imidazole solvate $[Mg_3\{(Im)BH_2(Im)\}_6(ImH)_6]\cdot ImH$ was obtained in form of white powder from $Mg(BH_4)_2$ and ImH melt. The yield was 53 % (1.2 g).

Structural Characterization of the Acetonitrile Solvate

Crystal structure of the acetonitrile solvate was successfully solved using single-crystal XRD from rod-shaped crystal with typical size of 50×200 µm. X-Ray structural analysis on single crystal has shown that the title compound is composed of Mg-based trimeric coordination molecules (Figure 1) parallel with crystallographic *c* direction and the solvent acetonitrile molecules.

The symmetry imposed by threefold inversion axis, which runs through Mg1 and Mg2 atoms, makes the coordination molecules linear. The distance between the neighboring Mg atoms (Mg1–Mg2) is 8.3753(6) Å. Each Mg is octahedrally coordinated with six nitrogen atom donors from imidazole moieties with the Mg–N distances between 2.1931(11) and 2.2060(12) Å.

The adjacent Mg atoms are connected *via* three *in-situ* formed bis(imidazolyl)borate bridging anions $\{(Im)BH_2(Im)\}^-$ which are representatives of poly(1-imidazolyl)borate family of ligands. Terminal Mg atoms are additionally coordinated with three monodentate

imidazole ligands resulting in formula $[Mg_3\{(Im)BH_2(Im)\}_6(ImH)_6]\cdot CH_3CN$.

Even though (1-imidazolyl)borates represent well-established ligand system (over 100 hits in the CSD[25]) to our knowledge only two structures containing ligands with unsubstituted imidazolates in the moiety $\{(Im)BH_2(Im)\}^-$, coordinated to metal ions via the nitrogen donors were described until now.[26] In the first (refcode QESTIR in the CSD[25]), the ligand is monodentate while in the second (refcode QESTUD) two bridging $\{(Im)BH_2(Im)\}^-$ ligands are present. In both compounds silver atoms serve as coordination centers and the coordination spheres of the central atoms are completed by assistance of phosphine-like ligands coordinated to Ag^+. Even though Mg-based trinuclear building units with linear geometry are commonly found in metal-organic framework structures, where adjacent Mg^{2+} centers are bridged via carboxylate ligands,[48] bridging through hybrid organic-borohydride species is a novelty.

In the compound described herein, the three bis(imidazolyl)borate bridges between the Mg^{2+} centers lead to the formation of characteristic cages with diameter of 4.6 Å, possibly capable of capturing/adsorbing selected species, that has not been observed previously (Figure S2 in the Supporting Information). Linear trinuclear coordination units with the length of ∼23 Å are packed in typical rhombohedral stacking, where the cylindrical $[Mg_3\{(Im)BH_2(Im)\}_6(ImH)_6]$ moieties align parallel along the c direction of the unit cell (with Mg atoms positioned on the threefold inversion axes), while the molecules of the same kind in the neighboring column are shifted by $\frac{1}{3}$ along c direction thus bringing together the parts of molecules, capable of forming moderately strong $BH\cdots HN$ polar interactions, which hold them together and stabilize the entire structure in pseudo 3-dimensional array (Figure S2 in the Supporting Information). Due to the shift of the neighboring columns along the c axis, voids are formed at each end of the molecules, which are filled with acetonitrile solvent in the analyzed form of the compound. The acetonitrile molecule is disordered as already described in Crystal structure optimizations in the Experimental Section and its role in the stability of the crystal is discussed below.

The title system in the form of acetonitrile solvate was inspected also by ^{1}H, ^{11}B and ^{13}C solid-state NMR spectroscopy (Figure 2). The carbon NMR spectrum is the most informative. It exhibits seven strong signals in the chemical shift range between 110 ppm and 150 ppm and a weak signal at about 1 ppm. The strong signals belong to carbon atoms of the three crystallographically distinct Im molecules. A quantitative measurement shows that the ratio of the relative intensities of these signals is approximately 1:1:1:1:2:2:1. This means that some carbon sites have very similar local environments, which lead to the overlap of the corresponding resonance lines. Detailed assignment of the resolved signals can be accomplished by the DFT/GIPAW calculations of isotropic chemical shifts, which are based on the structural model derived from the XRD analysis. The agreement between the calculated and the detected chemical shifts is quite good (Supplementary Information, Figure S3). It is worth noting that the carbon signals resonating at 117 ppm and 136 ppm are somewhat broader than the rest of the carbon NMR signals. These two signals belong to C1t and C3t atoms of the terminal, monodentatly bound Im unit. Broadening of these signals suggests that the positions (orientations) of the terminal ImH species are less well defined than the positions of the bridging, bidentately bound Im species. The weak carbon contribution resonating at about 1 ppm belongs to methyl carbon atoms of the acetonitrile molecules. Close inspection of this contribution shows that it is composed of more than one resonance line, thus suggesting that the acetonitrile molecules can adopt different orientations within the crystals of the compound.

^{11}B MAS NMR spectrum of the acetonitrile solvate exhibits one strong signal with a typical quadrupolar lineshape at about -10 ppm, and two weak signals resonating at 4 ppm and between 12 ppm and 20 ppm. Given that the structural model of the compound predicts a single boron environment and that the intensities of the latter two signals are much lower than the intensity of the signal at -10 ppm, the weak signals very likely belong to impurities, which are in a powdered sample present in a very low concentration. The quadrupolar parameters, determined by the analysis of the experimental boron NMR spectrum (C_{Q}=1.4 MHz,

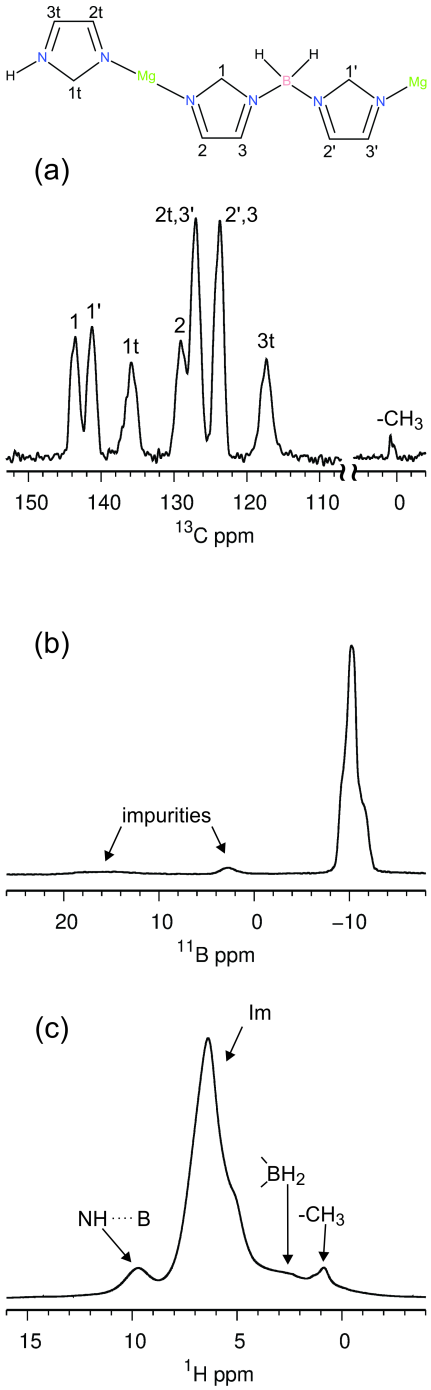

Figure 2: ^{1}H-^{13}C LG-CPMAS (a), ^{11}B MAS (b) and ^{1}H MAS (c) NMR spectra of the title system in the form of acetonitrile solvate. Assignment of carbon signals is based on first-principles calculations of isotropic chemical shifts, whereas assignment of hydrogen signals is based on heteronuclear-correlation NMR experiments and first-principles calculations. Scheme on top offers a key for the labeling of carbon signals.

η_Q=0.73), agree very well with the parameters calculated with the DFT/PAW calculations (C_Q=1.5 MHz, η_Q=0.70); this provides additional support to the proposed structural model.

^{1}H MAS NMR spectrum is the least resolved among the three NMR spectra. The most intense signal resonates at about 6.5 ppm and comprises contributions of hydrogen atoms of the three nonequivalent Im species. The assignment is clearly confirmed by the two-dimensional ^{1}H-^{13}C heteronuclear-correlation (HETCOR) NMR spectrum and by DFT/GIPAW calculations (Supplementary Information, Figure S4). The two-dimensional spectrum also shows that the relatively sharp ^{1}H NMR signal close to 1 ppm belongs to the methyl protons of the acetonitrile molecules. ^{1}H-^{11}B HETCOR experiment elucidates the origin of a low, broad signal extending between 2 ppm and 4 ppm (Supplementary Information, Figure S4); this signal belongs to hydrogen atoms attached to boron. The most difficult is the assignment of the well resolved signal at ∼9.7 ppm, as it does not exhibit any correlation peak in the above-described HETCOR spectra. Its chemical shift suggests that the signal could belong to protons in a moderately strong hydrogen bond. According to the proposed structural model, BH$\cdots$HN polar interactions exist between the N-H atoms of the terminal ImH species and the borohydride groups. Indeed, the DFT/GIPAW calculations predict the isotropic chemical shift of 10 ppm for these hydrogen nuclei, which again agrees very well with the observation.

From the results of geometry optimizations of the acetonitrile solvate crystal structure with three different functionals (Table S4 in the Supporting Information) it is apparent that functional RP shows the best agreement with experimental volume (discrepancy of 0.3 %). Unit cell dimensions of the optimized structure changed anisotropically relative to experimental data with parameter a changing for 0.02 % and parameter c for 0.29 %. This suggests that the structure is most sensitive to interaction changes in direction of axis c. Acetonitrile molecule is involved in many short contacts with neighboring molecules of $[Mg_3\{(Im)BH_2(Im)\}_6(ImH)_6]$. Predominant are of the type BH$\cdots$HC, where one methyl group bridges two BH_2 groups from different $[Mg_3\{(Im)BH_2(Im)\}_6(ImH)_6]$ molecules, thus providing additional cohesion between the main building units in the structure. Further-

more, dispersion interactions appear to importantly stabilize the structure, because when dispersion corrections are omitted, the optimized unit cell parameters increase dramatically (by more than 10 %; see Table S5 in the Supporting Information). Otherwise, regardless of the applied computational model, the agreement between computed and crystallographically determined atomic positions is very good, the computed interatomic distances and angles differing by less than 1 % from the respective experimental values (see Table S4 in the Supporting Information).

Optimizations of model structures with six different acetonitrile orientations resulted in similar structure energies. The difference between the highest and the lowest energy was 0.023 eV (2.2 kJ/mol) per one acetonitrile molecule, suggesting that the molecules are able to rotate around the threefold inversion axis virtually freely, since the energy differences are comparable to the thermal motion energy (k_BT) at room temperature. The structure with the most stable orientation of acetonitrile molecules was used in further calculations. Optimized atomic coordinates of an acetonitrile molecule in the optimized structure with the lowest energy were used in structure refinement process as described in the Experimental Section, Single Crystal X-ray Diffraction, since DFT methods provided more accurate information than diffraction due to crystallographic disorder.

Interaction energy of acetonitrile with coordination molecules, estimated by subtracting energy of acetonitrile molecule in vacuum (multiplied by the number of acetonitrile molecules in the unit cell) and energy of the model structure without acetonitrile molecules from the energy of crystallography-predicted structure with the lowest energy was −0.422 eV (−40.7 kJ/mol), normalized to a single acetonitrile molecule. Considering negative interaction energy and increase of optimized unit cell volume upon removal of acetonitrile, it can be concluded that acetonitrile stabilizes the structure with moderately strong polar interactions. In contrast to the observed difference of accuracy/sensitivity of the employed DFT approach between crystallographic axes, the volume increase on removal of the acetonitrile molecule from the already optimized structure appears to be quite isotropic, because all of

the unit cell vectors elongate by a comparable amount of 0.3–0.4 %. This suggests that the acetonitrile molecule stabilizes the structure almost equally in all spatial directions.

Stability, Purity and Sorption Properties of the Acetonitrile Solvate

Powder X-ray patterns of all solvothermally-obtained products and their single-crystal and powder fractions contained crystalline phase with the same structure as determined by single-crystal diffraction, while some samples also contained imidazole impurity (Figure 3). Imidazole polymorph with space group $P2_1/c$ was sometimes observed in the powder phase of samples. Powder patterns of crystals, formed on the surface of the liner, generally exhibited higher intensity peaks than patterns of the powder phase.

XRD scan of the acetonitrile solvate sample exposed to air confirmed that the compound is stable in air for at least one month at room conditions. This is in agreement with periodically recorded infrared spectra in Figure 4, which differ minimally from one another and indicate identical composition of the sample across the whole sampling timeline. Differences between the spectra are attributed to different sample loading and pressure applied during data acquisition, since they mostly manifest in form of slightly different peak intensities.

Even though $[Mg_3\{(Im)BH_2(Im)\}_6(ImH)_6]\cdot CH_3CN$ is defined as molecular structure, the described neighboring moieties are stacked through $BH\cdots HN$ polar interactions into pseudo 3-dimensional structure. Thermogravimetric analysis along with the temperature-programmed powder XRD shown in Figure 5 demonstrates the thermal behavior of the overall structure. Thermogravimetric curve basically shows four distinct weight losses in different temperature regimes. First loss below 60 °C can be assigned to the removal of the acetonitrile solvent located on the material's surface. Rapid drying process seen in the first step is followed by more gradual removal of acetonitrile involved in the material's crystal structure in the temperature region from 60 to 150 °C. Molecular structure and crystal packing seems to withstand the removal of solvent as indicated by XRD patterns measured up to 160 °C. Remaining two steps with similar weight contributions between 160 and 500 °C

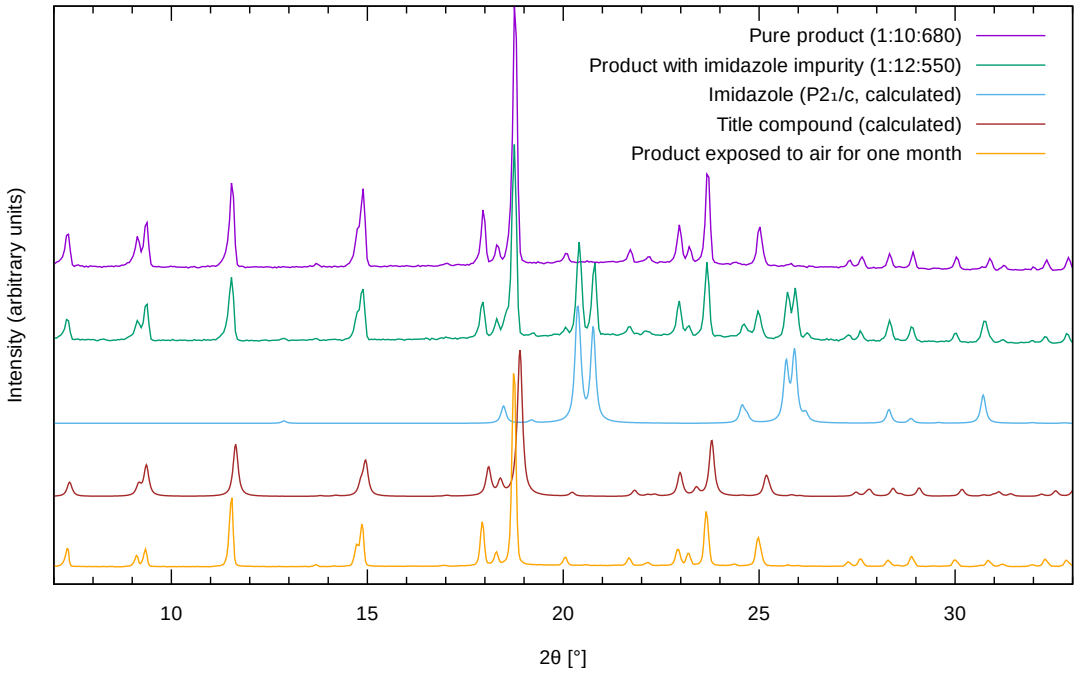

Figure 3: Powder X-ray patterns of pure and impure products, obtained by the solvothermal method, and product exposed to air for one month compared to calculated patterns of imidazole and the title compound in the form of acetonitrile solvate. Some patterns are scaled for ease of comparison. Slight mismatch between positions of measured and calculated peaks of the title compound is a consequence of different measurement temperatures. Molar ratios of reactants used to obtain the products are given in parentheses in order $Mg(BH_4)_2$, ImH, CH_3CN.

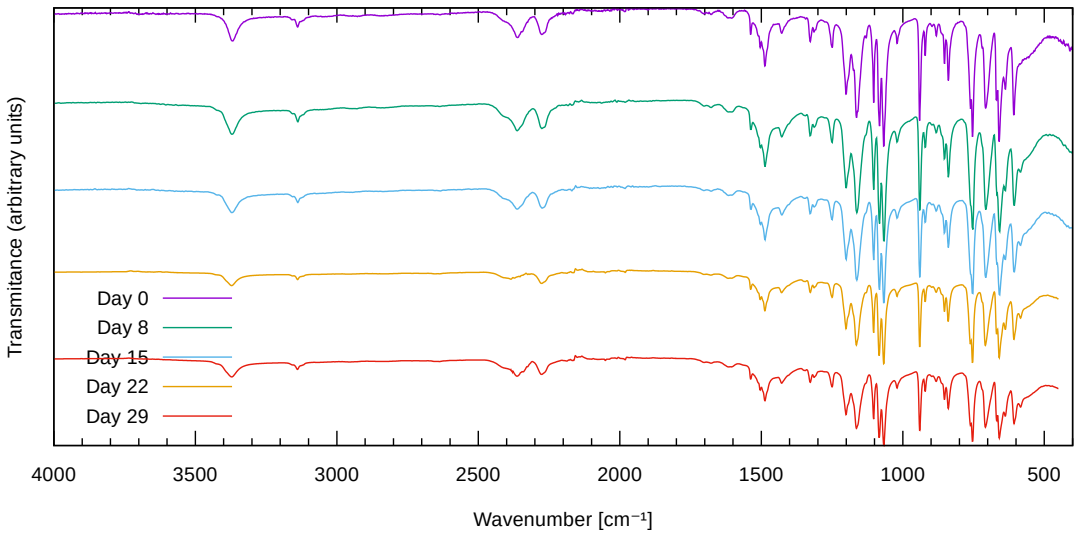

Figure 4: Periodically recorded infrared spectra of powdered sample of the acetonitrile solvate exposed to air.

are most probably due to the decomposition of protonated (terminal) and deprotonated (bridging) ligands together with the removal of BH_2 groups. Removal of ligand fragments is accompanied by substantial amorphisation of material.

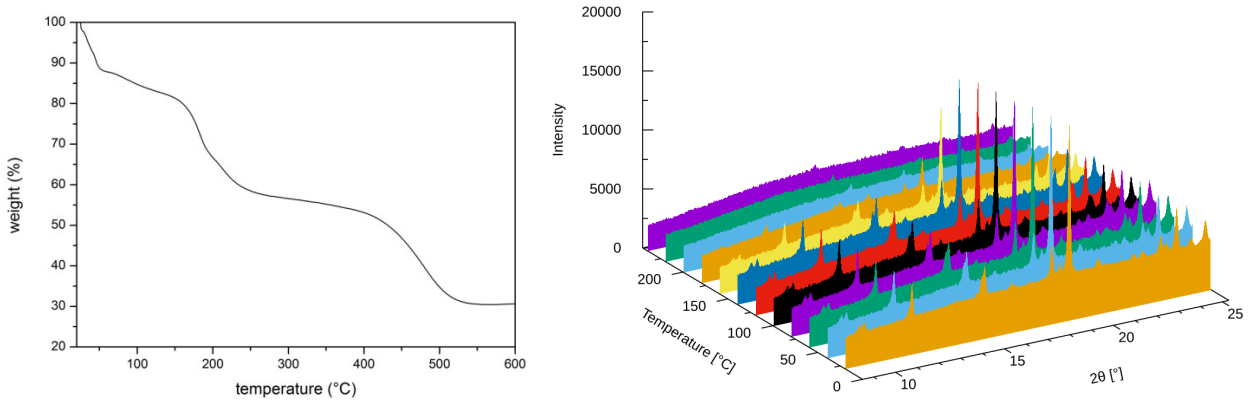

Figure 5: Thermogravimetric curve (left) and temperature-programmed XRD powder patterns (right), recorded from room temperature to 200 °C for every 20 °C, of $[Mg_3\{(Im)BH_2(Im)\}_6(ImH)_6] \cdot CH_3CN$.

As described above, the trinuclear molecular moieties form cages with diameter of 4.6 Å and can therefore potentially adsorb small gas molecules. Nevertheless N_2 sorption isotherms measured at 77 K show that these cages are not accessible for N_2 molecules. Material exhibits type III isotherm typical for nonporous adsorbents with negligible BET surface area of $9\,m^2/g$. The rapid increase of N_2 uptake occurs only above relative pressures 0.8 due to the N_2 condensation on the surface of the material. Similar effect can be observed for H_2 adsorption at 77 K with gradual near-linear increase of uptake up to 10 bar with no sign of saturation. The orientation of imidazolate ligands that form cages prevent the access of even smallest gas molecules to adsorb within the trinuclear moieties. N_2 and H_2 isotherms are available in the Supporting Information.

Characterization of the Imidazole Solvate

Temperature-programmed X-ray powder diffraction shows that the room temperature powder pattern of the title compound, prepared from the imidazole melt, is very similar to that

of the acetonitrile solvate (Figure 6), confirming the structural similarity. In contrast to the acetonitrile solvate, however, the imidazole solvate is stable up to 220 °C and transforms to another crystalline product upon thermal decomposition. The product is stable up to 360 °C. Conversely, acetonitrile solvate decomposes to an amorphous material at temperatures above 160 °C.

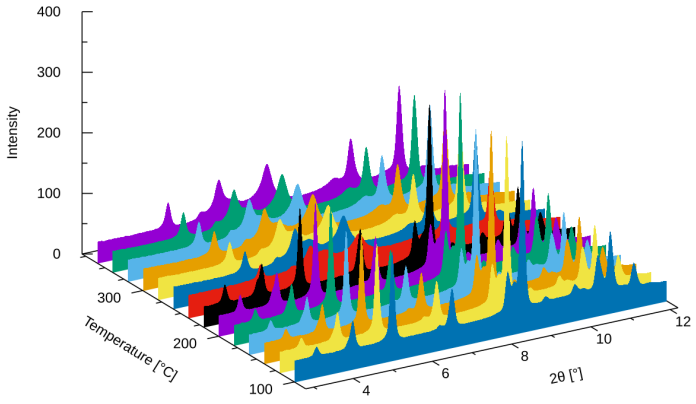

Figure 6: Synchrotron temperature-programmed XRD powder pattern of the imidazole solvate.

The material, synthesized in the imidazole melt, was expected to be a rather pure solvent-free form of the title compound. Its powder pattern was completely indexable by a rhombohedral unit cell, very similar to that of the acetonitrile solvate and its ^{11}B NMR spectrum in D_2O (see the Supporting Information) revealed only bi-substituted borohydride groups (BH_2) and a small amount of BH_4 impurity from $Mg(BH_4)_2$. However, it was proven by Rietveld refinement that this material does not consist of exclusively trinuclear $[Mg_3\{(Im)BH_2(Im)\}_6(ImH)_6]$ moieties. From difference Fourier map it was evident that there is missing electron density between these moieties (the space occupied by acetonitrile molecules in the acetonitrile solvate – see the Supporting Information).

By occupying the aforementioned space with the model of imidazole molecule, a very good Rietveld fit was achieved. The population parameter of imidazole was refined to 0.159, which is very close to the maximum possible of $\frac{1}{6}$ in regards to the 6-fold symmetry of the site, suggesting that the voids are nearly fully occupied. Similar refinements were performed

with patterns collected at 80 (see the Supporting Information), 160, 200 and 220 °C, and resulted in imidazole population parameters of 0.155, 0.154, 0.136 and 0.114, respectively, indicating that the voids are still 68 % occupied at the highest temperature, just before the structure disintegrates.

These findings confirm that formation and stability of the rhombohedral structure, built principally from $[Mg_3\{(Im)BH_2(Im)\}_6(ImH)_6]$ moieties, is solvent-dependent. On one hand, the solvent can be viewed as a spacer or void filler, fitting into the void between the trinuclear moieties, when they arrange in the rhombohedral manner so that BH_2 groups of one unit are close to NH groups of the neighboring ones to maintain $BH\cdots HN$ polar interactions. On the other hand, the solvent molecule is also involved in interactions with BH_2 groups of the surrounding molecules (Figure S10 in the Supporting Information). This seems to apply for both solvents studied and was also confirmed by DFT calculations for the case of acetonitrile.

Crystal Structure of $Mg(BHIm_3)_2$

The crystalline phase, formed by thermal decomposition of the imidazole solvate, generally exhibited broad and less reproducible peaks in powder XRD patterns. Despite that, omitting some inconsistent low intensity peaks, a trigonal unit cell ($a = 8.725$ Å, $c = 17.75$ Å, $V = 1170$ Å^3) was found using Dicvol.[49] Based on the shape and possible symmetries of the unit cell, chemical composition of the imidazole solvate structure, high-temperature conditions and structure density considerations multiple possible structural models were constructed. Among those were models containing $BHIm_3$ moieties, assuming a reaction between hydrogen atoms of terminal imidazole molecules of trinuclear moieties and hydrides of BH_2 bridges. Since there are several known structures containing the $BHIm_3$ moiety in the CSD, it was possible to construct a realistic model for such a structural fragment. Upon Rietveld refinement, one of the model structures readily converged to a reasonable arrangement (Figure 7) with an acceptable fit of the measured powder pattern. A detailed description

of the structure solution process and the Rietveld fit of the measured powder pattern are available in the Supporting Information.

The structure consists of layers, having the formula $Mg(BHIm_3)_2$, where Mg atoms are sandwiched between the $BHIm_3$ moieties so that the nitrogen imidazolate atoms, not bound to boron, form nearly regular octahedron around Mg. The layers are stacked in a primitive trigonal manner and there are no remarkable short contact between the layers (Figure 7). More data can be found in the Supporting Information.

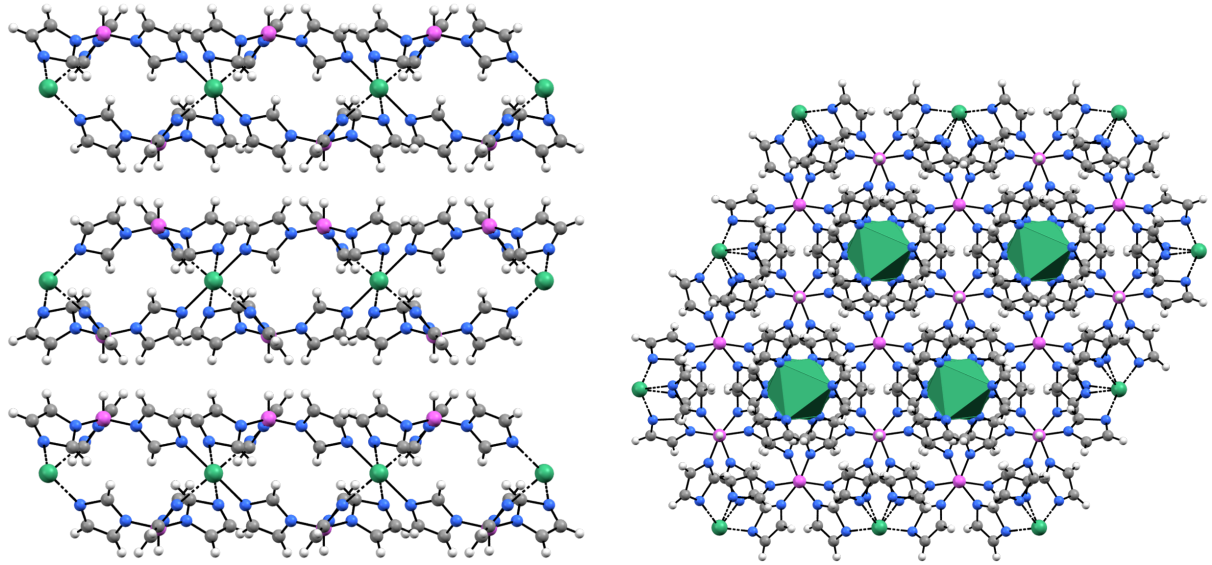

Figure 7: Packing of $Mg(BHIm_3)_2$ layers (left) and view of the same structure in the direction of layer stacking (right).

Conclusion

Aiming to produce compounds, consisting of metal coordination centers, imidazolate linkers and borohydride units, we first succeeded to synthesize a magnesium bis(imidazolyl)borate compound with the formula $[Mg_3\{(Im)BH_2(Im)\}_6(ImH)_6] \cdot CH_3CN$. The synthesis procedure was rather straightforward solvothermal treatment of magnesium borohydride and large excess of imidazole in acetonitrile. This enabled partial dehydrogenation of borohydride ions and deprotonation of part of imidazole molecules, which gave rise to in situ formation of

$\{(\mathrm{Im})\mathrm{BH_2}(\mathrm{Im})\}^-$ species. The latter coordinated in bridging mode to $\mathrm{Mg^{2+}}$ centers, producing trinuclear complex that adopted neutral imidazole molecules at both ends forming linear molecular moiety. To our best knowledge, such type of compound has not been reported yet.

The crystal structure of $[\mathrm{Mg_3}\{(\mathrm{Im})\mathrm{BH_2}(\mathrm{Im})\}_6(\mathrm{ImH})_6]\cdot\mathrm{CH_3CN}$ was determined by single-crystal X-ray diffraction and further elucidated by periodic DFT computational methods and solid state NMR, associated with GIPAW calculations. All results were in good agreement with each other.

The compound crystallizes in rather high-symmetry rhombohedral $\mathrm{R\bar{3}}$ space group and includes one disordered molecule of acetonitrile per one trinuclear complex in the voids between the trimeric $[\mathrm{Mg_3}\{(\mathrm{Im})\mathrm{BH_2}(\mathrm{Im})\}_6(\mathrm{ImH})_6]$ complexes. The complexes are arranged in rhombohedral stacking, where the polar interactions of the type $\mathrm{BH}\cdots\mathrm{HN}$ (between the negative hydride, bonded to boron and positive hydrogen, bonded to nitrogen) hold the complexes together in the lateral directions. Acetonitrile molecules fill the voids in between the complexes in the longitudinal direction and additionally stabilize the structure via $\mathrm{BH}\cdots\mathrm{HC}$ interactions.

Although the molecules $[\mathrm{Mg_3}\{(\mathrm{Im})\mathrm{BH_2}(\mathrm{Im})\}_6(\mathrm{ImH})_6]$ contain voids of the size of 4.6 Å between magnesium ions, sorption measurements indicated that voids between bis(imidazolyl)-borate bridges are inaccessible for even the smallest molecules, such as $\mathrm{H_2}$. This can be due to dense packing of the molecules, which does not allow diffusion of the molecular species to the voids even if they could eventually be filled.

It was found that the reported compound is stable at room conditions and its structure withstands heating up to 160 °C. Moderate thermal stability and nonsensitivity to humid conditions makes this material suitable for future investigations of its reactivity, due to two types of potentially reactive hydrogen atoms, hydride, bonded to boron, and hydrogen, bonded to nitrogen.

Synthesis from imidazole melt, aiming to produce a solvent-free product, led to imidazole solvate instead, proving that both acetonitrile and imidazole solvate molecules play an impor-

tant role in assisting a very similar rhombohedral packing of the $[Mg_3\{(Im)BH_2(Im)\}_6(ImH)_6]$ molecules. Imidazole solvate is more stable on heating and transforms to a new crystalline phase above 220 °C. The crystal structure of this new phase was solved from synchrotron powder diffraction data and shows that the discrete $[Mg_3\{(Im)BH_2(Im)\}_6(ImH)_6]$ molecules transform into infinite two-dimensional layers with a simple formula of $Mg(BHIm_3)_2$. The outcome proved that two types of reactive hydrogens in the same structure represent a potential for further transformations of this material. Particularly, the new layered structure was formed from the molecular one exactly by comproportionation of hydride, bound to boron, and hydrogen, bound to nitrogen.

The investigation described herein clearly proved the concept of integrating light-metal based imidazolates, coordinated via N atoms, and borohydrides, utilizing BH_2 bridging, within the same structure. This can lead to the development of a new generation hybrid materials for energy storage applications.

Acknowledgement

The authors thank Robert Cerović for preliminary syntheses. This work was supported by Slovenian Research Agency research programs P1-0012, P1-0021 and P1-0175. We thank the EN-FIST Center of Excellence, Ljubljana, Slovenia, for using SuperNova diffractometer.

The authors acknowledge the financial support of the Swiss National Science Foundation in the scope of Joint research projects (SCOPES) under the title "Metal-Hydride Organic Frameworks (HOF) – new solids for gas adsorption and separation".

We thank CSC for the fellowship for Xiao Li, FNRS for financial support and SNBL/ESRF staff for the support in measurements.

Supporting Information Available

The following files are available free of charge.

- supporting.pdf: Detailed synthesis procedure, additional crystallographic, NMR, sorption, and DFT data, detailed description of Rietveld refinements and additional figures of the crystal strutures.

CCDC 2017788, 2158335, and 2158345 contain the supplementary crystallographic data. These data can be obtained free of charge from The Cambridge Crystallographic Data Centre via `www.ccdc.cam.ac.uk/data_request/cif`.

References

(1) Díaz, U.; Brunel, D.; Corma, A. Catalysis using multifunctional organosiliceous hybrid materials. *Chem. Soc. Rev.* **2013**, *42*, 4083–4097.

(2) Lee, J.; Farha, O. K.; Roberts, J.; Scheidt, K. A.; Nguyen, S. T.; Hupp, J. T. Metal–organic framework materials as catalysts. *Chem. Soc. Rev.* **2009**, *38*, 1450–1459.

(3) Hoffmann, F.; Cornelius, M.; Morell, J.; Fröba, M. Silica-Based Mesoporous Organic–Inorganic Hybrid Materials. *Angew. Chemie Int. Ed.* **2006**, *45*, 3216–3251.

(4) Taguchi, A.; Schüth, F. Ordered mesoporous materials in catalysis. *Microporous Mesoporous Mater.* **2005**, *77*, 1–45.

(5) Centi, G.; Perathoner, S. Catalysis by layered materials: A review. *Microporous Mesoporous Mater.* **2008**, *107*, 3–15.

(6) Taylor-Pashow, K. M. L.; Della Rocca, J.; Huxford, R. C.; Lin, W. Hybrid nanomaterials for biomedical applications. *Chem. Commun.* **2010**, *46*, 5832–5849.

(7) Li, Z.; Barnes, J. C.; Bosoy, A.; Stoddart, J. F.; Zink, J. I. Mesoporous silica nanoparticles in biomedical applications. *Chem. Soc. Rev.* **2012**, *41*, 2590–2605.

(8) Cobo, I.; Li, M.; Sumerlin, B. S.; Perrier, S. Smart hybrid materials by conjugation of responsive polymers to biomacromolecules. *Nature Mater.* **2015**, *14*, 143–159.

(9) Owens, G. J.; Singh, R. K.; Foroutan, F.; Alqaysi, M.; Han, C.-M.; Mahapatra, C.; Kim, H.-W.; Knowles, J. C. Sol–gel based materials for biomedical applications. *Prog. Mater. Sci.* **2016**, *77*, 1–79.

(10) Li, J.; Zhang, J. Z. Optical properties and applications of hybrid semiconductor nanomaterials. *Coord. Chem. Rev.* **2009**, *253*, 3015–3041.

(11) Choi, H.; Yoon, H. Nanostructured Electrode Materials for Electrochemical Capacitor Applications. *Nanomaterials* **2015**, *5*, 906–936.

(12) Wang, S.; Kang, Y.; Wang, L.; Zhang, H.; Wang, Y.; Wang, Y. Organic/inorganic hybrid sensors: A review. *Sensors Actuators B Chem.* **2013**, *182*, 467–481.

(13) Pardo, R.; Zayat, M.; Levy, D. Photochromic organic–inorganic hybrid materials. *Chem. Soc. Rev.* **2011**, *40*, 672–687.

(14) Pomerantseva, E.; Bonaccorso, F.; Feng, X.; Cui, Y.; Gogotsi, Y. Energy storage: The future enabled by nanomaterials. *Science* **2019**, *366*, eaan8285.

(15) Khin, M. M.; Nair, A. S.; Babu, V. J.; Murugan, R.; Ramakrishna, S. A review on nanomaterials for environmental remediation. *Energy Environ. Sci.* **2012**, *5*, 8075–8109.

(16) Mendoza-Sánchez, B.; Gogotsi, Y. Synthesis of Two-Dimensional Materials for Capacitive Energy Storage. *Adv. Mater.* **2016**, *28*, 6104–6135.

(17) Hirscher, M. et al. Materials for hydrogen-based energy storage – past, recent progress and future outlook. *J. Alloy. Compd.* **2020**, *827*, 153548.

(18) Kadota, K.; Duong, N. T.; Nishiyama, Y.; Sivaniah, E.; Kitagawa, S.; Horike, S. Borohydride-containing coordination polymers: synthesis, air stability and dehydrogenation. *Chem. Sci.* **2019**, *10*, 6193–6198.

(19) Rossin, A.; Tuci, G.; Luconi, L.; Giambastiani, G. Metal–Organic Frameworks as Heterogeneous Catalysts in Hydrogen Production from Lightweight Inorganic Hydrides. *ACS Catal.* **2017**, *7*, 5035–5045.

(20) Sun, W.; Li, S.; Mao, J.; Guo, Z.; Liu, H.; Dou, S.; Yu, X. Nanoconfinement of lithium borohydride in Cu-MOFs towards low temperature dehydrogenation. *Dalton Trans.* **2011**, *40*, 5673–5676.

(21) Bhakta, R. K.; Herberg, J. L.; Jacobs, B.; Highley, A.; Behrens, R.; Ockwig, N. W.; Greathouse, J. A.; Allendorf, M. D. Metal–Organic Frameworks As Templates for Nanoscale $NaAlH_4$. *J. Am. Chem. Soc.* **2009**, *131*, 13198–13199.

(22) Andrew Lin, K.-Y.; Chen, S.-Y. Bromate reduction in water by catalytic hydrogenation using metal–organic frameworks and sodium borohydride. *RSC Adv.* **2015**, *5*, 43885–43896.

(23) Ingleson, M.; Barrio, J.; Bacsa, J.; Steiner, A.; Darling, G.; Jones, J.; Khimyak, Y.; Rosseinsky, M. Magnesium Borohydride Confined in a Metal–Organic Framework: A Preorganized System for Facile Arene Hydroboration. *Angew. Chem. Int. Ed.* **2009**, *48*, 2012–2016.

(24) Zhang, H.-X.; Liu, M.; Wen, T.; Zhang, J. Synthetic design of functional boron imidazolate frameworks. *Coordin. Chem. Rev.* **2016**, *307*, 255–266.

(25) Groom, C. R.; Bruno, I. J.; Lightfoot, M. P.; Ward, S. C. The Cambridge Structural Database. *ActaCryst.* **2016**, *B72*, 171–179.

(26) Effendy,; Gioia Lobbia, G.; Pellei, M.; Pettinari, C.; Santini, C.; Skelton, B. W.; White, A. H. Bridged poly(1-imidazolyl)borate silver(I) complexes containing tertiary mono(phosphine) ligands. The first structurally authenticated bis(imidazolyl)borate metal complex. *J. Chem. Soc., Dalton Trans.* **2001**, 528–534.

(27) Shuto, Y.; Yamamura, T.; Tanaka, S.; Yoshimura, M.; Kitamura, M. Asymmetric NaBH4 1,4-Reduction of C3-Disubstituted 2-Propenoates Catalyzed by a Diamidine Cobalt Complex. *ChemCatChem* **2015**, *7*, 1547–1550.

(28) Leiner, S.; Mayer, P.; Nöth, H. Synthesis and Structures of $LiBH_4$ Complexes with N-Heterocycles. *Z. Naturforsch.* **2009**, *64b*, 793–799.

(29) Morelle, F. Hybrid hydridic frameworks by the combination of complex hydrides and nitrogen-based organic ligands. Ph.D. thesis, Université catholique de Louvain, Louvain-la-Neuve, Belgium, 2017.

(30) Skripov, A. V.; Dimitrievska, M.; Babanova, O. A.; Skoryunov, R. V.; Soloninin, A. V.; Morelle, F.; Filinchuk, Y.; Faraone, A.; Wu, H.; Zhou, W.; Udovic, T. J. Low-Temperature Rotational Tunneling of Tetrahydroborate Anions in Lithium Benzimidazolate-Borohydride $Li_2(bIm)BH_4$. *J. Phys. Chem. C* **2019**, *123*, 20789–20799.

(31) CrysAlisPro. Agilent Technologies Ltd: Yarnton, Oxfordshire, England, Editon edn, 2014.

(32) Palatinus, L.; Chapuis, G. SUPERFLIP – a computer program for the solution of crystal structures by charge flipping in arbitrary dimensions. *J. Appl. Crystallogr.* **2007**, *40*, 786–790.

(33) Sheldrick, G. M. Crystal structure refinement with SHELXL. *Acta Cryst.* **2015**, *C71*, 3–8.

(34) Macrae, C. F.; Sovago, I.; Cottrell, S. J.; Galek, P. T. A.; McCabe, P.; Pidcock, E.; Platings, M.; Shields, G. P.; Stevens, J. S.; Towler, M.; Wood, P. A. *Mercury 4.0*: from visualization to analysis, design and prediction. *J. Appl. Cryst.* **2020**, *53*, 226–235.

(35) Kresse, G.; Hafner, J. Ab initio molecular dynamics for liquid metals. *Phys. Rev. B* **1993**, *47*, 558–561.

(36) Kresse, G.; Furthmüller, J. Efficiency of ab-initio total energy calculations for metals and semiconductors using a plane-wave basis set. *Comput. Mater. Sci.* **1996**, *6*, 15–50.

(37) Kresse, G.; Furthmüller, J. Efficient iterative schemes for ab initio total-energy calculations using a plane-wave basis set. *Phys. Rev. B* **1996**, *54*, 11169–11186.

(38) Kresse, G.; Hafner, J. Norm-conserving and ultrasoft pseudopotentials for first-row and transition elements. *J. Phys.: Condens. Matter* **1994**, *6*, 8245–8257.

(39) Hammer, B.; Hansen, L. B.; Nørskov, J. K. Improved adsorption energetics within density-functional theory using revised Perdew-Burke-Ernzerhof functionals. *Phys. Rev. B* **1999**, *59*, 7413–7421.

(40) Perdew, J. P.; Burke, K.; Ernzerhof, M. Generalized Gradient Approximation Made Simple. *Phys. Rev. Lett.* **1996**, *77*, 3865–3868.

(41) Grimme, S.; Antony, J.; Ehrlich, S.; Krieg, H. A consistent and accurate *ab initio* parametrization of density functional dispersion correction (DFT-D) for the 94 elements H-Pu. *J. Chem. Phys.* **2010**, *132*, 154104.

(42) Kresse, G.; Joubert, D. From ultrasoft pseudopotentials to the projector augmented-wave method. *Phys. Rev. B* **1999**, *59*, 1758–1775.

(43) Blöchl, P. E. Projector augmented-wave method. *Phys. Rev. B* **1994**, *50*, 17953–17979.

(44) Monkhorst, H. J.; Pack, J. D. Special points for Brillouin-zone integrations. *Phys. Rev. B* **1976**, *13*, 5188–5192.

(45) Björkman, T. CIF2Cell: Generating geometries for electronic structure programs. *Comput. Phys. Commun.* **2011**, *182*, 1183 – 1186.

(46) Csonka, G. I.; Perdew, J. P.; Ruzsinszky, A.; Philipsen, P. H. T.; Lebègue, S.; Paier, J.; Vydrov, O. A.; Ángyán, J. G. Assessing the performance of recent density functionals for bulk solids. *Phys. Rev. B* **2009**, *79*, 155107.

(47) Coelho, A. A. TOPAS and TOPAS-Academic: an optimization program integrating computer algebra and crystallographic objects written in C++. *J. Appl. Cryst.* **2018**, *51*, 210–218.

(48) Mazaj, M.; Kasunič, M.; Kaučič, V.; Logar Zabukovec, N. New Mg-based 4,4'-biphenyldicarboxylate Coordination Polymer with Layered Crystal Structure. *Acta Chim. Slov.* **2014**, *61*, 432–438.

(49) Boultif, A.; Louër, D. Indexing of powder diffraction patterns for low-symmetry lattices by the successive dichotomy method. *J. Appl. Cryst.* **1991**, *24*, 987–993.

TOC Graphic

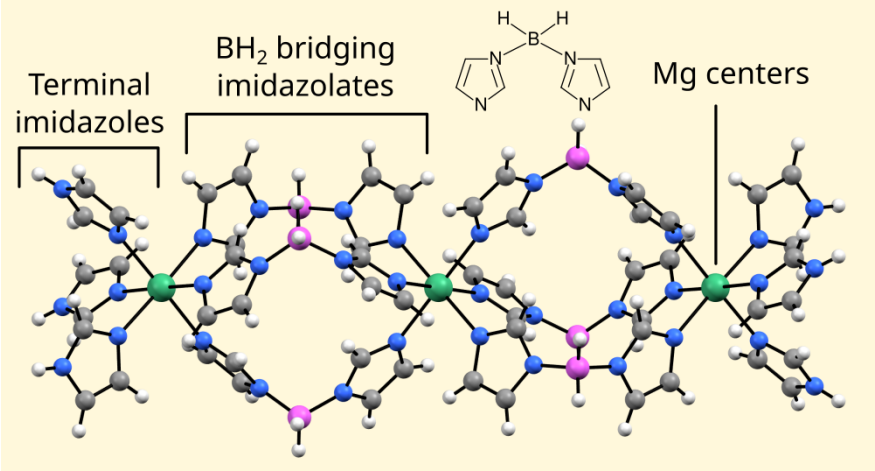

Synopsis

A trinuclear complex with magnesium centers, imidazolate-borohydride-imidazolate bridging ligands and imidazole terminal ligands was synthesized in the form of acetonitrile solvate and imidazole solvate. The compounds represent a rare case of imidazolyl borates where two potentially reactive hydrides remain on the boron. Heating of the title material leads to the release of hydrogen due to the comproportionation of borohydride and imidazole hydrogen atoms, resulting in a new layered structure of $Mg(BHIm_3)_2$.